International Journal of Microscale and Nanoscale Thermal ... ISSN: 1949-4955
Volume 2, Number 4

UNSTEADY MIXED CONVECTION FLOW FROM A MOVING VERTICAL SLENDER CYLINDER IN THE PRESENCE OF VISCOUS DISSIPATION

P. M. Patil[1], S. Roy[2], Ali J. Chamkha[*3], and P. S. Kulkarni[4]

[1]Department of Mathematics, J.S.S's Banashankari Arts,
Commerce and S. K. Gubbi Science College Vidyagiri, Dharwad,
Karnataka State, India
[2]Department of Mathematics, I.I.T Madras, Chennai, India
[3]Manufacturing Engineering Department,
The Public Authority for Applied Education and Training, Shuweikh, Kuwait
[4]Department of Aerospace Engineering, Indian Institute of Science, Bangalore, India

ABSTRACT

An unsteady mixed convection flow over a continuously moving vertical slender cylinder is considered to investigate the combined effects of buoyancy force and thermal as well as mass diffusion in presence viscous dissipation and surface mass transfer, where the slender cylinder is inline with the flow.

The unsteadiness in the flow, temperature and concentration fields is caused by the time dependent free stream velocity as well as by the continuously moving vertical slender cylinder.

The effect of surface curvature is also taken into account, particularly for the applications as wire and fiber drawing where exact predictions are expected. The governing boundary layer equations are transformed into a non-dimensional form by a special group of non-similar transformations. The resulting system of coupled non-linear partial differential equations is solved by an implicit finite difference scheme in combination with the quasi-linearization technique. Numerical computations are performed over the range of parameters ($0.7 \le \Pr \le 7.0$, $-0.41 \le \lambda \le 3.0$, $-1.0 \le N \le 1.0$, $-0.2 \le Ec \le 0.2$, $-2.0 \le A \le 2.0$, $0.22 \le Sc \le 2.57$, $0 \le \varepsilon \le 2.0$, $-0.75 \le \alpha \le 0.75$, $0 \le \xi \le 1$) display the velocity, temperature and concentration profiles graphically.

The numerical results for the local skin-friction coefficient, local Nusselt number and local Sherwood number are also presented. Present results are compared with previously published work and are found to be in excellent agreement.

Keywords: unsteady flow; mixed convection; slender cylinder; viscous dissipation; finite difference scheme; quasi-linearization technique

NOMENCLATURE

$A = \left(-R v_w / 4\nu\right)$, surface mass transfer parameter

C concentration

C_{fx} local skin friction coefficient

C_p specific heat at constant pressure

$Ec = \left(U_\infty^{\,2} / 4 C_P \left(T_{W0} - T_\infty\right)\right)$, Eckert number

f dimensionless stream function

F dimensionless velocity component

g acceleration due to gravity, m s^{-2}

G dimensionless temperature

$Gr_x = \left(g \beta_T \left(T_W\left(x\right) - T_\infty\right) x^3 / \nu^2\right)$, Grashof number due to temperature

$Gr_x^* = \left(g \beta_C \left(C_W\left(x\right) - C_\infty\right) x^3 / \nu^2\right)$, Grashof number due to concentration

H dimensionless concentration

$N = \left(\lambda^* / \lambda\right)$, ratio of Grashof numbers

Nu_x local Nusselt number

$Pr = \left(\nu / \alpha_m\right)$, Prandtl number

r radial coordinate, m

R radius of cylinder, m

$\mathrm{Re}_x = \left(U_\infty x / \nu\right)$, local Reynolds number

$Sc = \left(\nu / D\right)$, Schmidt number

Sh_x local Sherwood number

t dimensional time, s

T temperature, K

U_W moving plate velocity, m s^{-1}

U_∞ free stream velocity, m s^{-1}

u axial velocity component, m s^{-1}

v radial velocity component, m s^{-1}

x axial coordinate, m

Greek symbols

α unsteady parameter

α_m thermal diffusivity, m^2 s^{-1}

β_T, β_C volumetric coefficients of the thermal and concentration expansions, respectively, K^{-1}

ε wall velocity, m s^{-1}

τ dimensionless time

$\phi(\tau)$ unsteady function of τ

ξ transverse curvature

η non-dimensional co-ordinate

$\lambda = \left(Gr_x / \mathrm{Re}_x^{\,2}\right)$, buoyancy parameter (mixed convection) due to temperature gradient

$\lambda^* = \left(Gr_x^* / \mathrm{Re}_x^{\,2}\right)$, buoyancy parameter (mixed convection) due to concentration gradient

μ dynamic viscosity, $kg.m^{-1}s^{-1}$, Pa.s

ν kinematic viscosity, $m^2\ s^{-1}$

ρ density, $kg.m^{-3}$

ψ streamfunction

Subscripts

i initial condition

0 value at the wall for $\tau = 0$

w, ∞ conditions at the wall and infinity, respectively

x, r, *t* denote the partial derivatives with respect to these variables, respectively

ξ, η, τ denote the partial derivatives with respect to these variables, respectively

1. INTRODUCTION

A situation where both the forced and natural convection effects are of comparable order is known as mixed convection. Mixed convection flows, or combined forced and natural convection flows, arise in many transport processes both naturally and in engineering applications. They play an important role, for instance, in atmospheric boundary layer flows, heat exchangers, solar collectors, nuclear reactors and in electronic equipments. Such processes occur when the effects of buoyancy forces in forced convection or the effects of forced flow in natural convection become much more significant. The interaction of forced and natural convection is especially pronounced in physical situations where the forced flow velocity is low/ moderate and/ or the temperature differences are large.

Flows over cylindrical shaped bodies are often encountered in many thermal engineering applications such as cooling of rotating machinery, design of rotating heat exchanger, drying of paper etc. Flow over a cylinder is generally considered as two-dimensional as the radius of the cylinder is large enough compared to the boundary layer thickness while for a slender cylinder, if the radius of the cylinder is same as the order of the boundary layer thickness and then flow is considered to be axisymmetric. Thus, the flow may be considered as

axisymmetric instead of two-dimensional. In the axisymmetric flow, the governing equations consists of the transverse curvature term which is strong enough to induce the behavior of flow, temperature and concentration fields and correspondingly, the skin friction coefficient, heat and mass transfer rates over the surface.

The impact of transverse curvature is vital in many applications such as wire and fibre drawing wherein accurate prediction is expected and thick boundary layer can exist on slender or near slender bodies.

Unsteady mixed convection flows do not necessarily allow similarity solutions in many physical situations.

The nonsimilarity and unsteadiness in such flow problems may be due to the free stream velocity or due to the curvature of the body or due to the surface mass transfer or even possibly due to all these phenomenal effects. Since the mathematical difficulties involved in obtaining nonsimilar solutions for such problems, many researchers and scientists have confined their work either to steady nonsimilar flows or to unsteady semi similar or self similar flows [1-3].

Chen and Mucoglu [4] and Mucoglu and Chen [5] have investigated the effects of mixed convection over a vertical slender cylinder due to the thermal diffusion with prescribed wall temperature and heat flux conditions, respectively. They obtained the solution by using the local non-similarity method.

Further, Bui and Cebeci [6], Lee et al. [7] Wang and Kleinstruver [8], and more recently, Takhar et al. [9] have solved this problem using an implicit finite difference scheme. Heckel et al. [10] have discussed the variable temperature effects on the mixed convection flow over a vertical cylinder. Recently, Kumari and Nath [11] analyzed the effects of localized cooling/heating and suction/injection on the mixed convection flow on a thin vertical cylinder.

All the above studies are dealt with steady flows. In many practical situations, the flow could be unsteady due to the velocity of the moving cylinder which varies with time or due to the free stream velocity which also varies with time. Sparrow and Yu [12] have examined the local non-similarity thermal boundary layers. They have shown that when the ratio of the boundary layer thicknesses to the radius of the cylinder becomes greater than unity, the curvature effect enhances the heat transfer coefficient compared to that of characterizing the flat plate problem.

All the above studies are varying with time. Roy and Anilkumar [13] have investigated the unsteady effects on mixed convection flow over a moving vertical slender cylinder with surface mass transfer. Consequently, Singh et al [14] have examined the unsteady effects on mixed convection from a rotating vertical slender cylinder in an axial flow.

The objective of the present analysis is to obtain a non-similar solution of an unsteady mixed convection flow with combined effects of transverse curvature, viscous dissipation and thermal and mass diffusion over a continuously moving vertical cylinder, where the cylinder velocity and free stream velocity vary arbitrarily with time. The non-similar solutions are obtained numerically by solving a set of coupled nonlinear partial differential equations governing the mixed convection flow, by using the method of quasi-linearization in combination of an implicit finite difference scheme [15].

The numerical results for particular cases of the present results have been compared to those of Chen and Mucoglu [4], Takhar et al. [9] and Roy and Anilkumar [13] and they are found to be in excellent agreement.

2. ANALYSIS

Consider the unsteady mixed convection flow over a heated vertical moving slender cylinder with surface mass transfer. The blowing rate is assumed to be small and does not affect the inviscid flow at the edge of the boundary layer. The physical model and coordinate system are shown in Figure 1. The unsteadiness in the flow field is introduced by the moving slender cylinder velocity as well as free stream velocity, which vary with time. The radial coordinate r is measured from the axis of the cylinder and the axial coordinate x is measured vertically upward such as x = 0 corresponds to the leading edge. The radius of the slender cylinder is same as the order of the boundary layer thickness. Hence, the flow is taken to be axisymmetric. Thermophysical properties of the fluid in the flow model are assumed to be constant except the density variations causing a body force term in momentum equation. The Boussinesq approximation is invoked for the fluid properties to relate density changes to temperature changes, and to couple in this way the temperature field to the flow field [16]. Under these assumptions, the equation of conservation of mass, momentum, energy and concentration governing the mixed convection boundary layer flow over a moving vertical slender cylinder can be expressed as [13, 17]:

$$\frac{\partial}{\partial x}(ru) + \frac{\partial}{\partial r}(rv) = 0, \tag{1}$$

$$\frac{\partial u}{\partial t}+u\frac{\partial u}{\partial x}+v\frac{\partial u}{\partial r}=\frac{\partial u_e}{\partial t}+\frac{\nu}{r}\frac{\partial}{\partial r}\left(r\frac{\partial u}{\partial r}\right) \pm g\,\beta_T(T-T_\infty)\pm g\,\beta_C(C-C_\infty), \tag{2}$$

$$\frac{\partial T}{\partial t}+u\frac{\partial T}{\partial x}+v\frac{\partial T}{\partial r}=\frac{\alpha_m}{r}\frac{\partial}{\partial r}\left(r\frac{\partial T}{\partial r}\right)+\frac{\nu}{C_P}\left(\frac{\partial u}{\partial r}\right)^2, \tag{3}$$

$$\frac{\partial C}{\partial t}+u\frac{\partial C}{\partial x}+v\frac{\partial C}{\partial r}=\frac{D}{r}\frac{\partial}{\partial r}\left(r\frac{\partial C}{\partial r}\right), \tag{4}$$

The initial conditions are:

$$u(x,r,0)=u_i(x,r), v(x,r,0)=v_i(x,r),\ T(x,r,0)=T_i(x,r),$$
$$C(x,r,0)=C_i(x,r) \tag{5}$$

The physical boundary conditions for the problem are given by:

$$u(x,R,t)=U_W(t)=U_w\phi(\tau),\ v(x,R,t)=V_W,\ T(x,R,t)=T_W,\ C(x,R,t)=C_W,$$
at r = R
$$u(x,\infty,t)\to u_e(t)\to U_\infty\phi(\tau),\ T(x,\infty,t)\to T_\infty,\ C(x,\infty,t)\to C_\infty, \text{ as } r\to\infty, \tag{6}$$

where $\phi(\tau)=1+\alpha\tau^2$; $\alpha < 0$ or $\alpha > 0$.

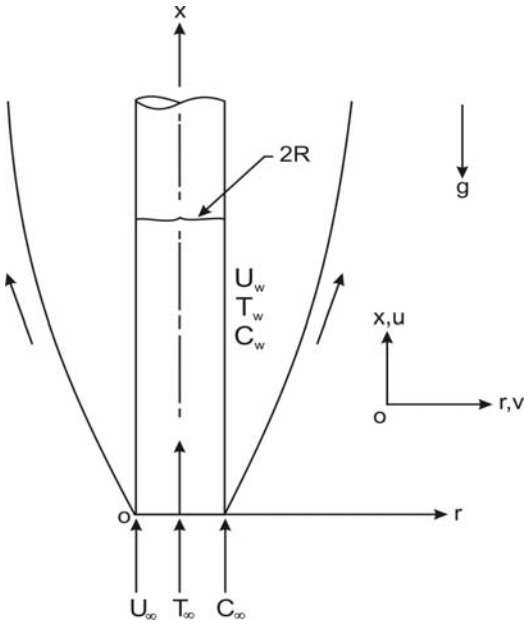

Figure 1. Physical model and coordinate system.

Applying the transformations:

$$\xi = \left(\frac{4}{R}\right)\left(\frac{\nu x}{U_\infty}\right)^{1/2};\ \eta = \left(\frac{U_\infty}{\nu x}\right)^{1/2}\left[\frac{r^2 - R^2}{4R}\right];\ \tau = \frac{\nu}{R^2}t;\ \frac{r^2}{R^2} = 1 + \xi\eta;$$

$$u = \frac{1}{r}\frac{\partial \psi}{\partial r};$$

$$v = -\frac{1}{r}\frac{\partial \psi}{\partial x};\psi(x,r,t) = R(\nu U_\infty x)^{1/2}\phi(\tau) f(\xi,\eta,\tau);$$

$$f_\eta(\xi,\eta,\tau) = F(\xi,\eta,\tau);\ u = \frac{1}{2}U_\infty \phi(\tau) F;$$

$$v = \frac{R}{2r}\phi\left(\frac{\nu U_\infty}{x}\right)^{1/2}\left[\eta f_\eta - f - \xi f_\xi\right];$$

$$G(\xi,\eta,\tau) = \frac{T - T_\infty}{T_W(x) - T_\infty};\ T_W(x) - T_\infty = (T_{W0} - T_\infty)x^{-1};$$

$$H(\xi,\eta,\tau) = \frac{C - C_\infty}{C_W(x) - C_\infty};$$

$$C_W(x) - C_\infty = (C_{W0} - C_\infty)x^{-1};\ Ec = \frac{{U_\infty}^2}{4C_P(T_{W0} - T_\infty)};\ \mathrm{Pr} = \frac{\nu}{\alpha_m};\ Sc = \frac{\nu}{D};$$

$$\lambda = \frac{Gr_x}{\mathrm{Re}_x^{\,2}}; \lambda^* = \frac{Gr_x^*}{\mathrm{Re}_x^{\,2}}; \; N = \frac{\lambda^*}{\lambda};$$

$$Gr_x = \frac{g\beta_T\left(T_W(x) - T_\infty\right)x^3}{\nu^2}; Gr_x^* = \frac{g\beta_C\left(C_W(x) - C_\infty\right)x^3}{\nu^2}; \; \mathrm{Re}_x = \frac{U_\infty x}{\nu}; \tag{7}$$

to Eqs. (1) to (4), we find that Eq. (1) is identically satisfied, and Eqs. (3) - (4) reduce to

$$\left[(1+\xi\eta)F_\eta\right]_\eta + \phi(\tau) f F_\eta + 8\lambda\phi^{-1}(\tau)(G + NH) + \left(\frac{\xi^2}{4}\right)\left[\phi^{-1}(\tau)\frac{d\phi(\tau)}{d\tau}(2-F) - F_\tau\right] = \phi(\tau)\xi\left[F F_\xi - F_\eta f_\xi\right] \tag{8}$$

$$\left[(1+\xi\eta)G_\eta\right]_\eta + \mathrm{Pr}\,\phi(\tau) f G_\eta + \mathrm{Pr}(1+\xi\eta)Ec\,\phi^2(\tau)F_\eta^{\,2} - \mathrm{Pr}\left(\frac{\xi^2}{4}\right)G_\tau = \mathrm{Pr}\,\phi(\tau)\xi\left[F G_\xi - G_\eta f_\xi\right], \tag{9}$$

$$\left[(1+\xi\eta)H_\eta\right]_\eta + Sc\,\phi(\tau) f H_\eta - Sc\left(\frac{\xi^2}{4}\right)H_\tau = Sc\,\phi(\tau)\xi\left[F H_\xi - H_\eta f_\xi\right]. \tag{10}$$

The reduced boundary conditions are

$$F(\xi,0,\tau) = \varepsilon, \; G(\xi,0,\tau) = 1, \; H(\xi,0,\tau) = 1, \; 0 \le \tau, \xi \le 1, \text{ at } \eta = 0, \tag{11}$$

$$F(\xi,\infty,\tau) \to 2, \; G(\xi,\infty,\tau) \to 0, \quad H(\xi,\infty,\tau) \to 0, \; 0 \le \tau, \xi \le 1 \text{ as } \eta \to \infty. \tag{12}$$

where, $\varepsilon = 2\left(\frac{U_W}{U_\infty}\right)$ and $f(\xi,\eta,\tau) = \int_0^\eta F dx + f_W$, $f_W = -\frac{R v_w \xi}{4\nu\phi} = \frac{A\xi}{\phi}$, (13)

$$A = -\frac{R v_w}{4\nu} = \text{constant}. \tag{14}$$

We have assumed that the flow is steady at time $\tau = 0$ and becomes unsteady for $\tau > 0$ due to the time dependent cylinder velocity $\left[U_W(t) = U_{w,0}\phi(\tau)\right]$ and free stream velocity $\left[u_e(t) = U_\infty\phi(\tau)\right]$, where $\phi(\tau) = 1 + \alpha\tau^2$; $\alpha < 0$ or $\alpha > 0$. Hence, the initial condition (i.e. conditions at $\tau = 0$) are given by the steady state equations obtained from (7) and (8) by substituting $\phi(\tau) = 1$, $d\phi/d\tau = F_\tau = G_\tau = H_\tau = 0$ when $\tau = 0$. The corresponding boundary conditions are obtained from (11-12).

The main physical quantities of interest are the skin friction coefficient $\left(C_{fx}\,\mathrm{Re}_x^{1/2}\right)$, the local Nusselt number $\left(Nu_x\,\mathrm{Re}_x^{-1/2}\right)$ and local Sherwood number $\left(Sh_x\,\mathrm{Re}_x^{-1/2}\right)$ which represent the wall shear stress, the heat transfer rate and mass transfer rate at the surface, respectively.

The local skin friction coefficient C_{fx} is defined as

$$C_{fx}=\mu\frac{2\left[\frac{\partial u}{\partial r}\right]_w}{\rho U^2}=2^{-1}\,\mathrm{Re}_x^{-\frac{1}{2}}\,\phi(\tau)\,F_\eta\left(\xi,0,\tau\right)_w, \tag{15}$$

$$\text{i.e. } C_{fx}\,\mathrm{Re}_x^{\frac{1}{2}}=2^{-1}\,\phi(\tau)\,F_\eta\left(\tau,\xi,0\right)_w. \tag{16}$$

The local heat transfer rate in terms of Nusselt number can be expressed as

$$Nu_x=-\frac{\left[x\frac{\partial T}{\partial r}\right]_w}{\left(T_w(x)-T_\infty\right)}=-2^{-1}\,\mathrm{Re}_x^{\frac{1}{2}}\,G_\eta\left(\xi,0,\tau\right)_w, \tag{17}$$

$$\text{i.e. } Nu_x\,\mathrm{Re}_x^{-\frac{1}{2}}=-2^{-1}\,G_\eta\left(\tau,\xi,0\right)_w. \tag{18}$$

The local mass transfer rate in terms of Sherwood number can be expressed as

$$Sh_x=-\frac{\left[x\frac{\partial C}{\partial r}\right]_w}{\left(C_w(x)-C_\infty\right)}=-2^{-1}\,\mathrm{Re}_x^{\frac{1}{2}}\,H_\eta\left(\xi,0,\tau\right)_w, \tag{19}$$

$$\text{i.e. } Sh_x\,\mathrm{Re}_x^{-\frac{1}{2}}=-2^{-1}\,H_\eta\left(\tau,\xi,0\right)_w. \tag{20}$$

3. METHOD OF SOLUTION

The non-linear coupled partial differential Eqs. (8) - (10) under the boundary conditions (11-12) have been solved numerically using an implicit finite difference scheme in combination with the quasi-linearization technique [14, 15].

Quasi-linearization technique can be viewed as a generalization of the Newton-Raphson approximation technique in functional space. An iterative sequence of linear equations is

carefully constructed to approximate the nonlinear Eqs. (8) - (10) under the boundary conditions (11-12) achieving quadratic convergence and monotonicity.

With the help of quasi-linearization technique, the nonlinear coupled partial differential Eqs. (8) - (10) with boundary conditions (11-12) are replaced by the following sequence of linear ordinary differential equations.

$$F_{\eta\eta}^{\,i+1} + X_1^{\,i} F_\eta^{\,i+1} + X_2^{\,i} F^{i+1} + X_3^{\,i+1} F_\xi^{\,i+1} + X_4^{\,i} F_\tau^{\,i+1} + X_5^{\,i} G^{i+1} + X_6^{\,i} H^{i+1} = X_7^{\,i}, \tag{21}$$

$$G_{\eta\eta}^{\,i+1} + Y_1^{\,i} G_\eta^{\,i+1} + Y_2^{\,i} G_\xi^{\,i+1} + Y_3^{\,i} G_\tau^{\,i+1} + Y_4^{\,i} F^{i+1} + Y_5^{\,i} F_\eta^{\,i+1} = Y_6^{\,i}, \tag{22}$$

$$H_{\eta\eta}^{\,i+1} + Z_1^{\,i} H_\eta^{\,i+1} + Z_2^{\,i} H_\xi^{\,i+1} + Z_3^{\,i} H_\tau^{\,i+1} + Z_4^{\,i} F^{i+1} = Z_5^{\,i}, \tag{23}$$

The coefficient function with iterative index i are known and the function with iterative index (i+1) are to be determined. The corresponding boundary conditions are given by

$$F^{i+1}(\xi, 0, \tau) = \varepsilon, \qquad G^{i+1}(\xi, 0, \tau) = 1, \qquad H^{i+1}(\xi, 0, \tau) = 1,$$
$$\text{at } \eta = 0, \tag{24}$$

$$F^{i+1}(\xi, \eta_\infty, \tau) = 2, \qquad G^{i+1}(\xi, \eta_\infty, \tau) = 0, \qquad H^{i+1}(\xi, \eta_\infty, \tau) = 0,$$
$$\text{at } \eta = \eta_\infty. \tag{25}$$

where η_∞ is the edge of the boundary layer and the coefficients in equations (21) - (23) are given in the Appendix. Since the method is presented for ordinary differential equations by Inouye and Tate [15] and also presented for partial differential equations in a recent study by Singh and Roy [14], its detailed description is not provided here. At each iteration step, the sequence of linear partial differential equations (21) – (23) were expressed in difference form using central difference scheme in the η- direction and backward difference scheme in ξ and τ directions. Thus in each step, the resulting equations were then reduced to a system of linear algebraic equations with a block tri-diagonal matrix, which is solved by Varga's algorithm [18]. To ensure the convergence of the numerical solution to the accurate solution, step sizes $\Delta\eta$, $\Delta\xi$ and $\Delta\tau$ are optimized and taken as 0.005, 0.01 and 0.01, respectively. The results presented here are independent of the step sizes at least up to the fourth decimal place. A convergence criterion based on the relative difference between the current and previous iteration values is employed. When the difference reaches 0.0001, the solution is assumed to have converged and the iteration process is terminated.

4. RESULTS AND DISCUSSION

The computations have been carried out for various values of $\mathrm{Pr}(0.7 \le \mathrm{Pr} \le 7.0)$, $\lambda(-0.41 \le \lambda \le 3.0)$, $\varepsilon(0 \le \varepsilon \le 2.0)$, $N(-1.0 \le N \le 1.0)$, $\alpha(-0.75 \le \alpha \le 0.75)$,

$\xi\left(0 \le \xi \le 1\right)$, $Sc\left(0.22 \le Sc \le 2.57\right)$, $A\left(-2.0 \le A \le 2.0\right)$ and $Ec\left(-0.2 \le Ec \le 0.2\right)$. The edge of the boundary layer $\left(\eta_\infty\right)$ has been taken between 2.8 and 5.0 depending on the values of the parameters. The results have been obtained for both accelerating $\left[\phi\left(\tau\right)=1+\alpha\tau^2;\alpha>0,\ 0\le\tau\le1\right]$ and decelerating $\left[\phi\left(\tau\right)=1+\alpha\tau^2;\alpha<0,\ 0\le\tau\le1\right]$ free stream velocities of the fluid. In order to verify the accuracy of the presented approach, we have verified steady state results of skin friction and heat transfer coefficients $\left[F_\eta\left(\xi,0\right),\ -G_\eta\left(\xi,0\right)\right]$ by direct comparison with the results previously reported by Chen and Mucoglu [4], Takhar et al. [9] and Roy and Anilkumar [13] and found them in excellent agreement. The results of this comparison are presented in Table 1 and are found to be in excellent agreement.

The effects of buoyancy parameter $\left(\lambda\right)$ and Prandtl number (*Pr*) on velocity and temperature profiles $\left(F\left(\xi,\eta,\tau\right),G\left(\xi,\eta,\tau\right)\right)$ for accelerating flow $\phi\left(\tau\right)=1+\alpha\tau^2$, $\alpha=0.5$, when *Ec* = 0.01, ε = 0.5, Sc = 0.22, N = 0.5, $A=1.0$ and $\xi=0.5$ are displayed in Figures 2 and 3. The action of buoyancy assisting force $\left(\lambda>0\right)$ shows the overshoot in the velocity profiles $F\left(\xi,\eta,\tau\right)$ near the wall for lower Prandtl number (*Pr*) fluid (air, *Pr* = 0.7) while for higher Prandtl number (*Pr*) fluid (water, *Pr* = 7.0), the velocity overshoot is not observed as shown in Figure 2.

The magnitudes of the velocity overshoot increases with buoyancy parameter $\left(\lambda>0\right)$ while it decreases as Prandtl number (*Pr*) increases. The physical reason is that the buoyancy force effect is larger in a smaller Prandtl number (*Pr*) fluid (air, *Pr* = 0.7) due to the lower viscosity of the fluid, which enhances the velocity profile within the moving boundary layer as the assisting buoyancy force acts like a favorable pressure gradient and the velocity overshoot occurs.

For higher Prandtl number (*Pr*) fluids (water, *Pr* = 7.0), the overshoot is not present because higher Prandtl number (*Pr*) fluids implies more viscous fluid which have less impact on the buoyancy parameter $\left(\lambda\right)$.

It is worthy to note from the Figures 2 and 3 that the buoyancy opposing force (λ < 0) reduces the magnitude of the velocity near the wall significantly within the moving boundary layer for lower Prandtl number fluids (*Pr* = 0.7, air) as well as for higher Prandtl number fluids (*Pr* = 7.0, water). The effect of time τ is crucial for the velocity overshoot. In particular, for $\alpha=0.5$, *Ec* = 0.5, ε = 1.0, Sc = 0.22, N = 0.5, $A=1.0$, $\xi=0.5$ at Pr = 0.7 when λ = 3.0, overshoot in the velocity profile reduced approximately by 35% as time τ increases from 0.0 to 1.0. The buoyancy parameter $\left(\lambda\right)$ has relatively less impact on the temperature profile $G\left(\xi,\eta,\tau\right)$ as shown in Figure 3. Furthermore, Figure 3 also shows that the higher Prandtl number fluids (water, *Pr* = 7.0) results into a thinner thermal boundary layer since the higher Prandtl number (*Pr*) fluids (water, *Pr* = 7.0) have a lower thermal conductivity.

Table 1. Comparison of the steady state results $\left(f_{\eta\eta}(\xi,0),-G_{\eta}(\xi,0)\right)$ with those of Chen and Mucoglu [4], Takhar et al. [9] and Roy and Anilkumar [13]

ξ	λ	Present results		Chen and Mucoglu [4]		Takhar et al. [9]		Roy and Anilkumar [13]	
		$f_{\eta\eta}(\xi,0)$	$-G_{\eta}(\xi,0)$	$f_{\eta\eta}(\xi,0)$	$-G_{\eta}(\xi,0)$	$f_{\eta\eta}(\xi,0)$	$-G_{\eta}(\xi,0)$	$f_{\eta\eta}(\xi,0)$	$-G_{\eta}(\xi,0)$
0	0	1.3282	0.5854	1.3282	0.5854	1.3281	0.5854	1.3282	0.5854
0	1	4.9665	0.8220	4.9666	0.8221	4.9663	0.8219	4.9664	0.8220
0	2	7.7123	0.9305	7.7126	0.9305	7.7119	0.9302	7.7122	0.9304
1	0	1.9170	0.8667	1.9172	0.8669	1.9167	0.8666	1.9169	0.8666
1	1	5.2583	1.0620	5.2584	1.0621	5.2578	1.0617	5.2580	1.0621
1	2	7.8873	1.1687	7.8871	1.1690	7.8863	1.1685	7.8871	1.1688

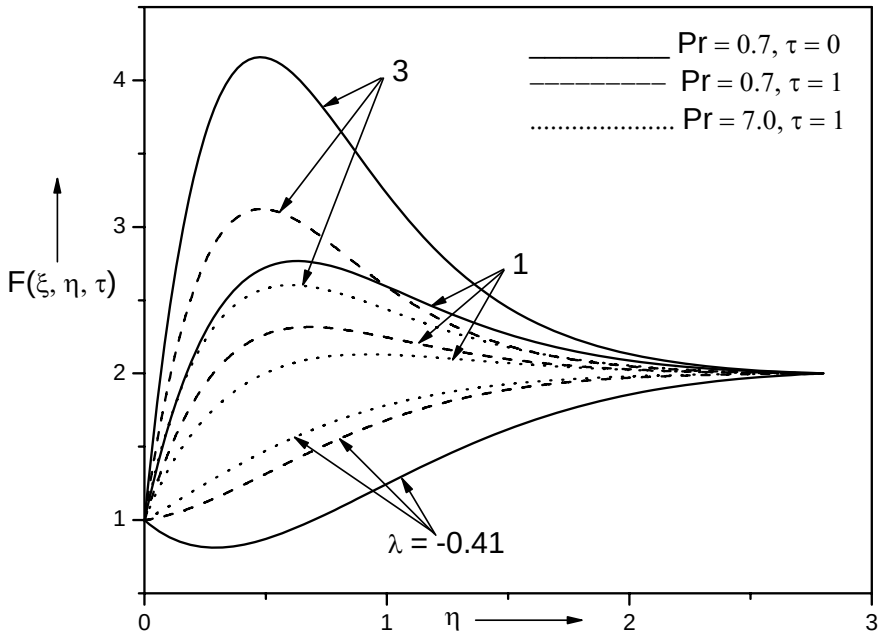

Figure 2. Effects of λ and Pr on velocity profile for $\phi(\tau)=1+\alpha\tau^2$, α = 0.5 when N = 0.5, Ec = 0.01, A = 1, ε = 1, Sc = 0.22 and ξ = 0.5.

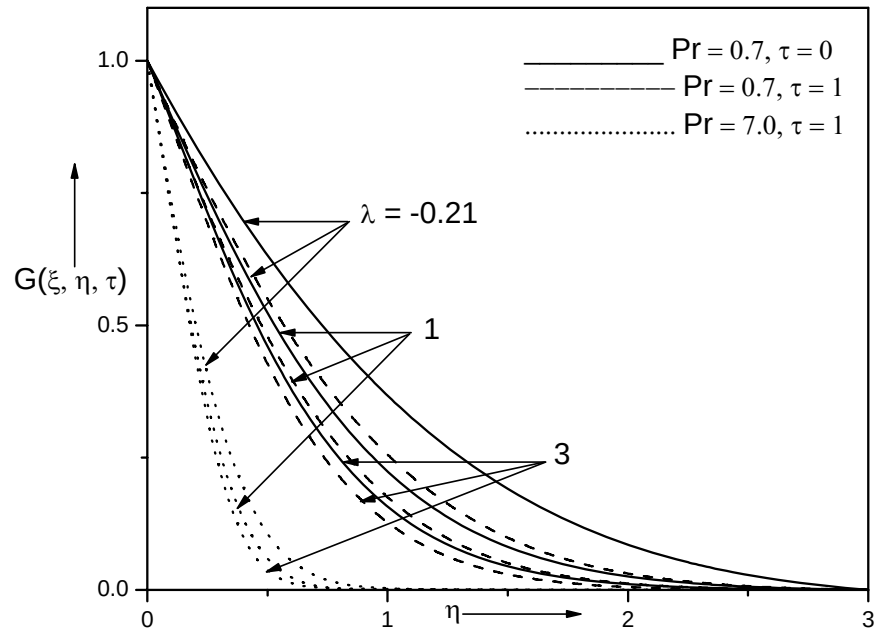

Figure 3. Effects of λ and Pr on temperature profile for $\phi(\tau)=1+\alpha\tau^2$, α = 0.5 when N = 0.5, Ec = 0.01, A = 0, ε = 1, Sc = 0.22 and ξ = 0.5.

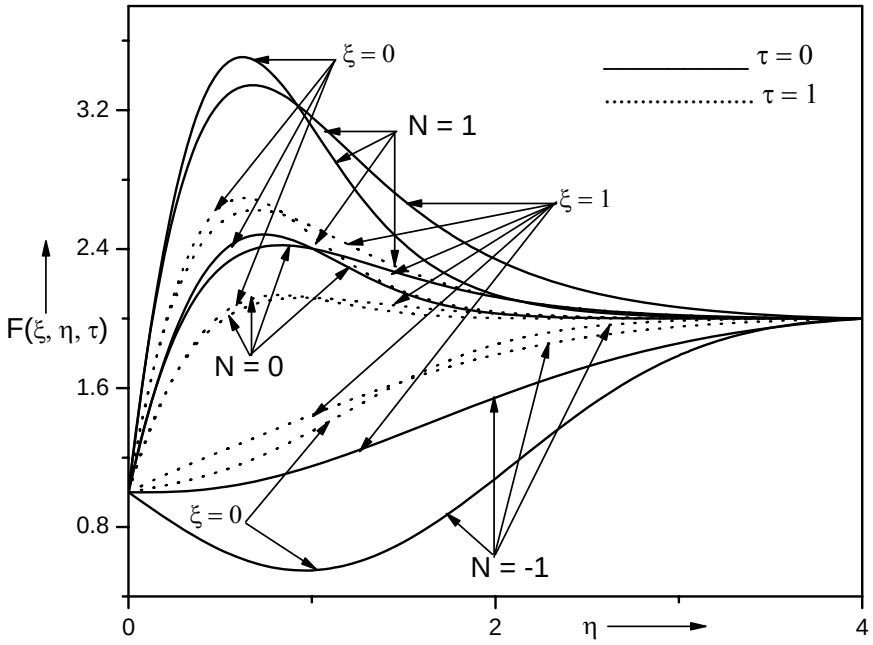

Figure 4. Effects of N and ξ on velocity profile for $\phi(\tau)=1+\alpha\tau^2$, α = 0.5 when λ = 1, Ec = 0.1, A = 0, ε = 1.0, Sc = 0.22.

Figure 4 illustrates the role of surface curvature parameter ξ and the ratio of buoyancy forces N on the velocity profile $F(\xi,\eta,\tau)$ for accelerating flow $\phi(\tau)=1+\alpha\tau^2$, $\alpha=0.5$, when *Ec* = 0.1, ε = 1.0, Sc = 0.22 , $A=0.0$, $\lambda=1.0$ and *Pr* = 0.7.

The ratio of buoyancy parameter (N>0) shows the presence of overshoot in the velocity profiles near the wall for the steady case $(\tau=0)$. Although, the magnitude of the overshoot increases with the ratio of buoyancy forces parameter $N(N>0)$, it decreases as the dimensionless time τ increases from 0.0 to 1.0. The physical reason is that the ratio of buoyancy forces parameter *N* affects more in steady case $(\tau=0)$. Hence, the velocity increases within the moving boundary layer as the assisting buoyancy force acts like a favorable pressure gradient and the velocity overshoot occurs. However, it is important to note from the Figure 4 that the ratio of buoyancy opposing forces (N < 0) reduces the magnitude of the velocity near the wall significantly within the moving boundary layer for the steady case $(\tau=0)$ as well as unsteady case $(\tau\neq0)$. Due to increase in the surface curvature parameter ξ, the steepness in the velocity profile $F(\xi,\eta,\tau)$ decreases in the vicinity of the wall but the magnitude of the velocity overshoot increases away from the wall as it can be seen from Figure 4. Hence, velocity profile $F(\xi,\eta,\tau)$ is decreasing with the increase of surface curvature parameter ξ as well as time τ from 0.0 to 1.0.

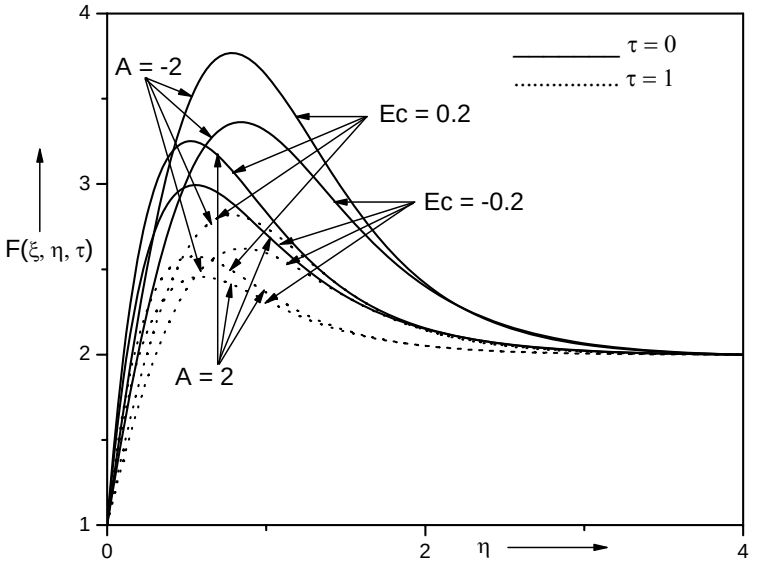

Figure 5. Effects of Ec and A on velocity profile for $\phi(\tau)=1+\alpha\tau^2$, α = 0.5 when λ = 1, ξ = 0.5, Pr = 0.7, N = 1, Sc = 0.22 and ε = 1.

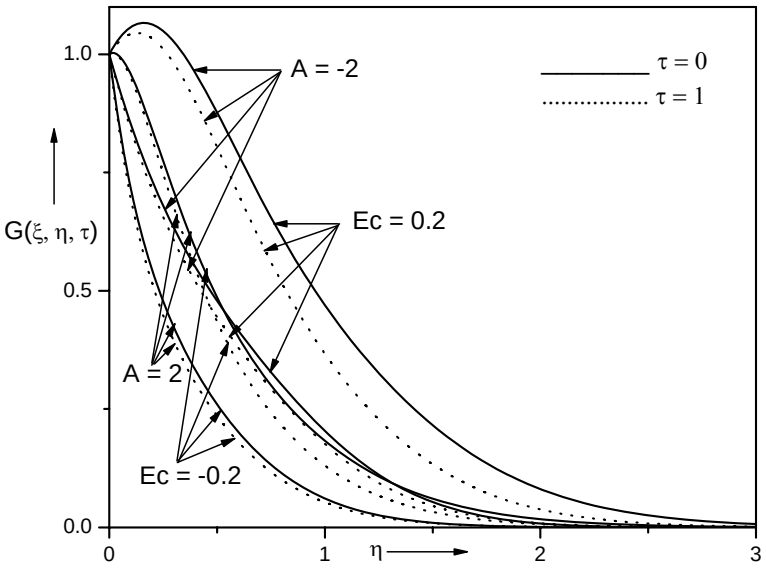

Figure 6. Effects of Ec and A on temperature profile for $\phi(\tau)=1+\alpha\tau^2$, α = 0.5 when λ = 1, ξ = 0.5, Pr = 0.7, N = 1, Sc = 0.22 and ε = 1.

The overshoot near the plate reduces with time τ . For example, *Ec* = 0.1, ε = 1.0, Sc = 0.22, $A=0.0$, $\lambda=1.0$, *Pr* = 0.7 and N = 1.0 at $\xi=1$ overshoot in the velocity profile reduced approximately by 24% as τ increases from 0.0 to 1.0.

Figures 5 and 6 depict the relative importance of the surface mass transfer A $(A>0 \text{ or } A<0)$ and viscous dissipation parameter Ec on the velocity and temperature profiles $\left(F(\xi,\eta,\tau), G(\xi,\eta,\tau)\right)$ for accelerating flow $\phi(\tau)=1+\alpha\tau^2$, $\alpha=0.5$, when ε = 1.0, N = 1.0, Sc = 0.22, $\lambda=1.0$, Pr = 0.7 and $\xi=0.5$.

In case of injection $(A<0)$, the fluid is carried away from the surface, causing reduction in the slope of the velocity as it tries to maintain the same velocity over a very small region near the surface, and this effect is quite reversed in the case of suction $(A>0)$.

The higher velocity overshoot is observed near the wall within the boundary layer for injection $(A<0)$ and overshoot is decreased for suction $(A>0)$. Injection $(A<0)$ causes a decrease in the steepness of the velocity profile $F(\xi,\eta,\tau)$ near the wall within the boundary layer, but the steepness of the velocity profile $F(\xi,\eta,\tau)$ increases with suction. The effects of viscous dissipation parameter of the fluid heating case (Ec = 0.2), exhibits that the velocity and temperature profiles are larger than that of the case without viscous dissipation (Ec = 0), whereas the opposite trend is observed for the fluid cooling case (Ec = - 0.2). The overshoot of the velocity and temperature profiles reduce with viscous dissipation parameter Ec = - 0.2. Also, the velocity and temperature overshoot reduce significantly at τ = 1.0. For example, $\alpha=0.5$, ε = 1.0, Sc = 0.22, N = 1.0, $\lambda=1.0$, *Pr* = 0.7 at $\xi=0.5$ when Ec = 0.2 overshoot in the velocity and temperature profiles reduced approximately by 25% and 12% respectively, as τ increases from 0.0 to 1.0.

Figure 7 displays the effects of wall velocity ε and time τ on the velocity profile $F(\xi,\eta,\tau)$ for $\phi(\tau)=1+\alpha\tau^2$, $\alpha=0.5$ and $\alpha=-0.5$ when λ = 1.0, *N* = 1.0, Sc = 0.22, *A* = 1.0, ξ = 0.5, *Ec* = 0.1 and *Pr* = 0.7. The velocity profile is strongly depending on ε because it occurs in the boundary condition for $F(\xi,\eta,\tau)$. It has been observed that the magnitude of the velocity within the moving boundary layer increases with the increase of ε while decreases as τ increases from τ = 0.0 to τ = 1.0. The physical reason is that the assisting buoyancy forces due to thermal and mass gradients as well as increase in ε acts like a favorable pressure gradient which accelerates the fluid for uniform motion when τ = 0.0 (steady case) causing the velocity overshoot near the surface within the moving boundary layer. The velocity overshoot reduces significantly at τ = 1.0 and also with the increase of ε. Furthermore, it is observed that the velocity profile increases with time τ within the moving boundary layer for decelerating flow $\phi(\tau)=1+\alpha\tau^2;\alpha=-0.5$. For example, λ = 1.0, *N* = 0.5, Sc = 0.22, ξ = 0.5, *Ec* = 0.1, *A* = 1.0 and *Pr* = 0.7 when $\varepsilon=2.0$ at ξ = 0.5, the velocity profile increases approximately about 55% when time τ increases from 0 to 1. This clearly indicates that the effect of moving boundary on the decelerating flow is very prominent.

Figures 8 and 9 illustrate the influence of the Schmidt number (Sc) and time τ on velocity and concentration profiles $\left(F(\xi,\eta,\tau), H(\xi,\eta,\tau)\right)$ for accelerating and

decelerating flows $\phi(\tau)=1+\alpha\tau^2, \alpha=\pm 0.5$, when ε = 1.0, λ = 1.0, N = 1.0, Pr = 0.7, $A=1.0$, Ec = 0.1 and $\xi=0.5$.

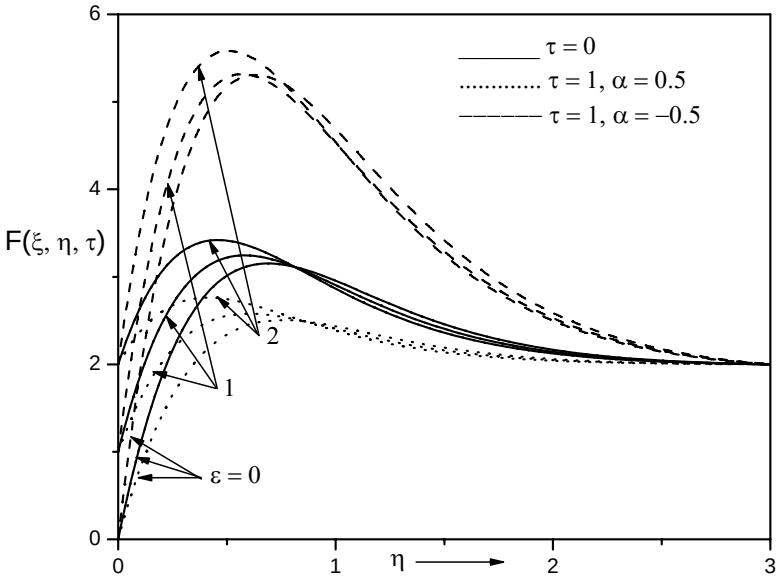

Figure 7. Effects of ε and τ on velocity profile for $\phi(\tau)=1+\alpha\tau^2$, α = 0.5 when λ = 1, ξ = 0.5, Pr = 0.7, N = 1, Sc = 0.22, Ec = 0.1 and A = 1.

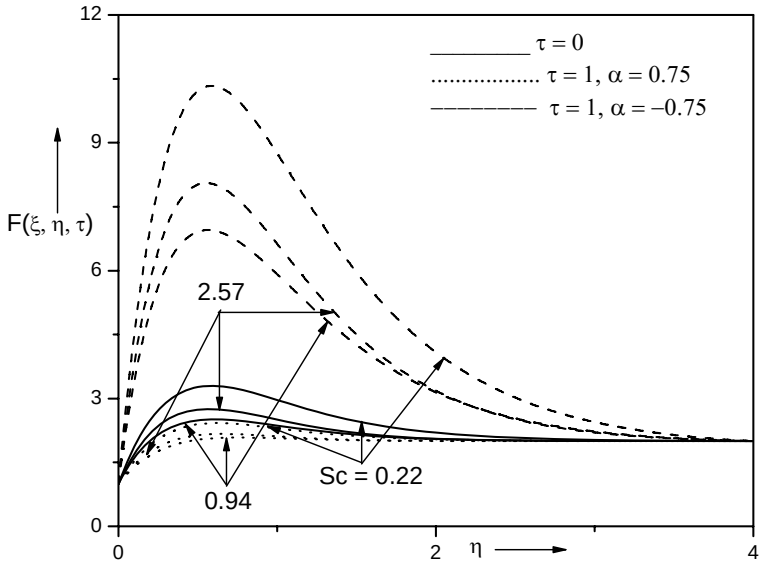

Figure 8. Effects of Sc and τ on velocity profile for $\phi(\tau)=1+\alpha\tau^2$, α = 0.5 when λ = 1, ξ = 0.5, Pr = 0.7, N = 1, Ec = 0.1, ε = 1 and A = 1.

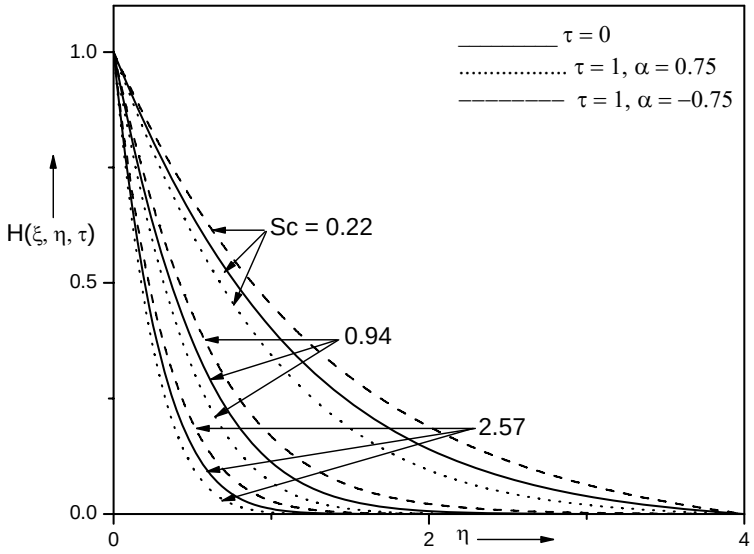

Figure 9. Effects of Sc and τ on concentration profile for $\phi(\tau)=1+\alpha\tau^2$, α = 0.5 when λ = 1, ξ = 0.5, Pr = 0.7, N = 1, Ec = 0.1, ε = 1 and A = 1.

The values of the Schmidt number (*Sc*) are chosen to be more realistic, 0.22, 0.94 and 2.57, representing diffusing chemical species of most common interest like water, Propyl Benzene hydrogen, water vapor and Propyl Benzene, etc., at 25 degree Celsius at one atmospheric pressure. It is observed that the velocity and concentration boundary layers are to decrease as the Schmidt number *Sc* is increased.

The physical reason is that the Schmidt number *Sc* leads to a thinning of the concentration boundary layer. As a result the concentration of the fluid decreases and this leads to a decrease in the fluid velocity. Further, the effect of decelerating flow is more pronounced on velocity and concentration profiles for low Schmidt number fluids (*Sc* = 0.22). Figures 8 displays that for *Sc* = 0.22, velocity profile has approximately 213 % more overshoot with a thick concentration boundary layer due to low mass diffusivity as time τ increases from 0.0 to 1.0.

Figures 10 and 11 represent the influence the effects of buoyancy parameter (λ) and surface curvature parameter ξ of accelerating and decelerating free stream flows ($\phi(t^*)=1+\alpha t^{*2}$, $\alpha=0.6$ or $\alpha=-0.6$) on the skin friction coefficient and heat transfer rate $\left(C_{fx}\,\mathrm{Re}_x^{1/2}, Nu_x\,\mathrm{Re}_x^{-1/2}\right)$ when *Ec* = 0.01, ε = 1.0, $A=1.0$, Sc = 2.57, N = 0.5 and *Pr* = 0.7.

Results reveal that $\left(C_{fx}\,\mathrm{Re}_x^{1/2}, Nu_x\,\mathrm{Re}_x^{-1/2}\right)$ increase with the increase of buoyancy parameter (λ). The physical reason is that the buoyancy force $(\lambda>0)$ implies favorable pressure gradient, and the fluid gets accelerated, which results in thinner momentum and thermal boundary layers. When surface curvature parameter ξ increases from 0.0 to 1.0, the

local Nusselt number $\left(Nu_x \operatorname{Re}_x^{-1/2}\right)$ increases as well skin friction coefficient $\left(C_{fx} \operatorname{Re}_x^{1/2}\right)$ increases, as shown in Figs. 10 and 11. For example, for $\alpha = 0.6$, Ec = 0.01, ε = 1.0, $A = 1.0$, Sc = 2.57, N = 0.5 and Pr = 0.7 when τ = 0.5, $\left(C_{fx} \operatorname{Re}_x^{1/2}\right)$ decreases approximately about 85% and 68% as λ decreases from 1.5 to 0.0 at $\xi = 0.0$ and at $\xi = 1.0$ (see Figure 10), respectively. Further, Figure 11 shows that $\left(Nu_x \operatorname{Re}_x^{-1/2}\right)$ increases approximately about 17% and only 2%, respectively, at ξ = 0 and at ξ = 1 when λ increases from 0.0 to 1.5. However, it is noted that in the case of accelerating flows, the heat transfer rate $\left(Nu_x \operatorname{Re}_x^{-1/2}\right)$ and skin friction coefficient $\left(C_{fx} \operatorname{Re}_x^{1/2}\right)$ increases with increasing time τ and $\left(Nu_x \operatorname{Re}_x^{-1/2}\right)$ and $\left(C_{fx} \operatorname{Re}_x^{1/2}\right)$ decreases with increasing time τ for the case of decelerating flows.

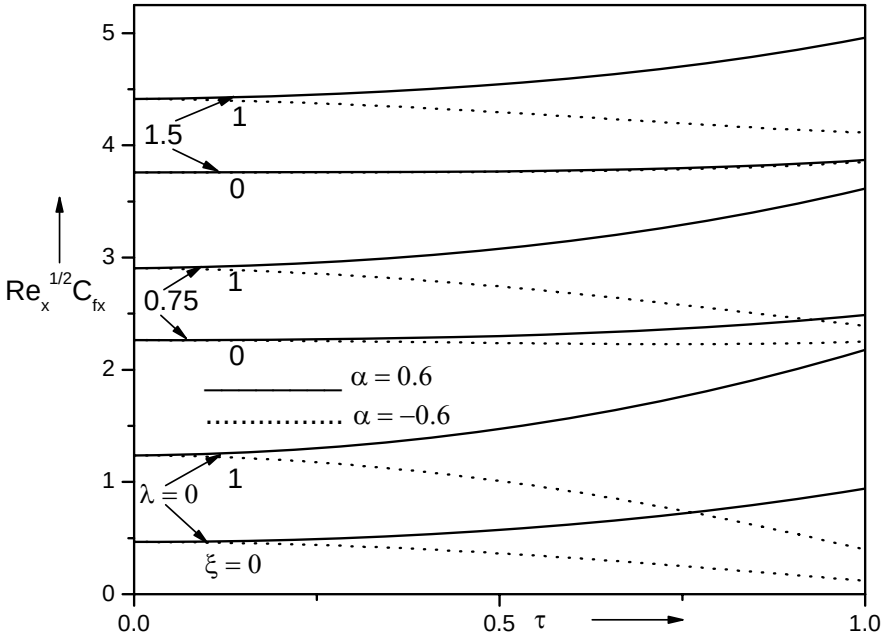

Figure 10. Effects of λ and ξ on skin friction coefficient for $\phi(\tau) = 1 + \alpha \tau^2$, when N = 0.5, Pr = 0.7, ε = 1, Sc = 2.57, Ec = 0.01 and A = 1.

Figure 12 displays the relative influence of accelerating and decelerating free stream flows ($\phi(\tau) = 1 + \alpha \tau^2$, $\alpha = 0.75$ or $\alpha = -0.75$) on the skin friction coefficient $\left(C_{fx} \operatorname{Re}_x^{1/2}\right)$ when Ec = 0.01, ε = 1.0, $A = 1.0$, Sc = 2.57, $\lambda = 1.0$ and ξ = 1.0. Results indicate that $\left(C_{fx} \operatorname{Re}_x^{1/2}, Nu_x \operatorname{Re}_x^{-1/2}\right)$ increase with the increase of ratio of buoyancy forces parameter (N).

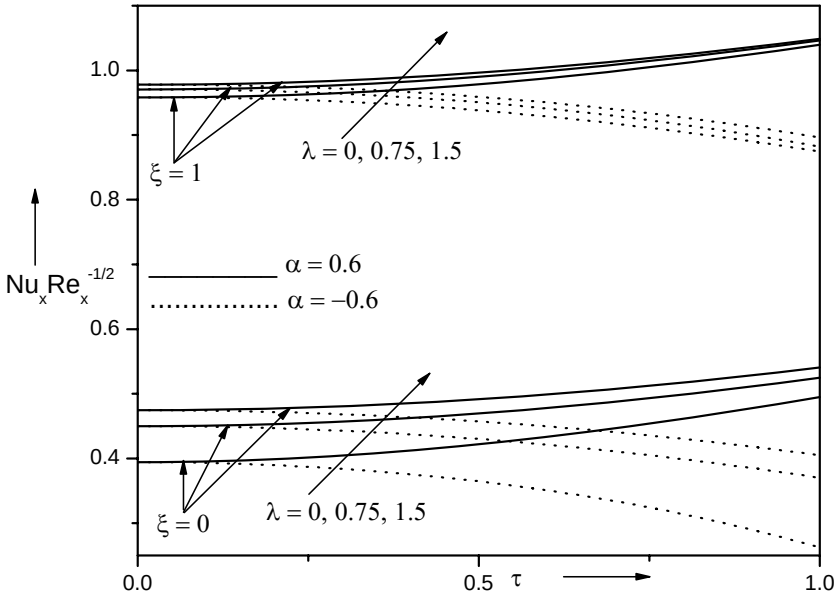

Figure 11. Effects of λ and ξ on heat transfer rate for $\phi(\tau)=1+\alpha\tau^2$, when N = 0.5, Pr = 0.7, ε = 1, Sc = 2.57, Ec = 0.01 and A = 1.

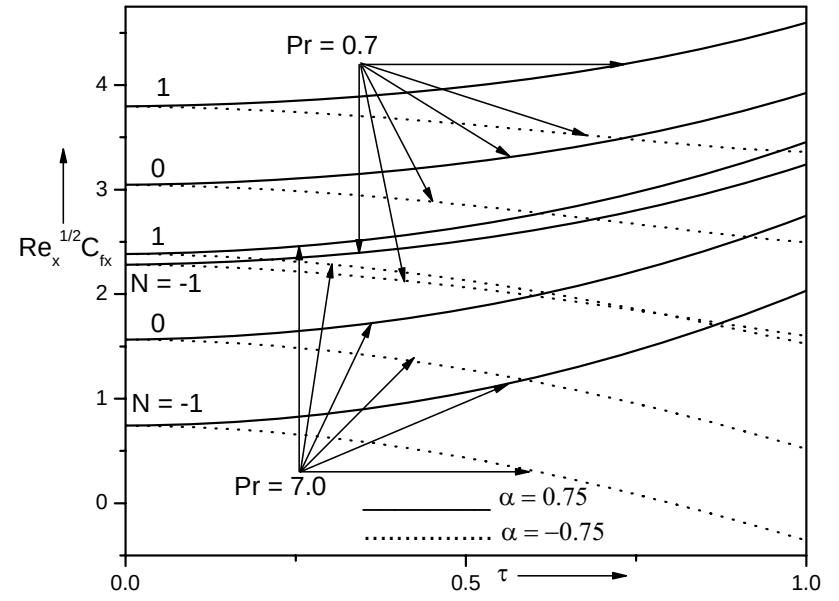

Figure 12. Effects of N and Pr on skin friction coefficient for $\phi(\tau)=1+\alpha\tau^2$, when ξ = 1, λ = 1, Sc = 2.57, Ec = 0.01, ε = 1 and A = 1.

The physical reason is that the ratio of buoyancy forces $(N>0)$ implies favorable pressure gradient, and the fluid gets accelerated, which results in thinner momentum

boundary layer. When Prandtl number Pr increases from 0.7 to 7.0, the local skin friction coefficient $\left(C_{fx}\,\mathrm{Re}_x^{1/2}\right)$ decreases, as shown in Figs. 12. For example, for $\alpha = 0.75$, *Ec* = 0.01, ε = 1.0, $A = 1.0$, *Sc* = 2.57, $\lambda = 1.0$ and ξ = 1.0 when τ = 0.5, $\left(C_{fx}\,\mathrm{Re}_x^{1/2}\right)$ increases approximately about 23% and 42% as N increases from 0.0 to 1.0 at *Pr* = 0.7 and at *Pr* = 7.0 (see Figure 12), respectively whereas $\left(C_{fx}\,\mathrm{Re}_x^{1/2}\right)$ decreases approximately about 23% and 43% as *N* decreases from 0.0 to -1.0 at *Pr* = 0.7 and at *Pr* = 7.0 (see Figure 12), respectively. Further, the skin friction coefficient $\left(C_{fx}\,\mathrm{Re}_x^{1/2}\right)$ increases with the increase of time τ for accelerating flows while in the case of decelerating flows, $\left(C_{fx}\,\mathrm{Re}_x^{1/2}\right)$ decreases with the increase of time τ as can be seen in Figure 12.

Figure 13 shows that effects viscous dissipation parameter *Ec* and Prandtl number Pr on heat transfer rate $\left(Nu_x\,\mathrm{Re}_x^{-1/2}\right)$ accelerating and decelerating free stream flows ($\phi(\tau) = 1 + \alpha\tau^2$, $\alpha = 0.75$ or $\alpha = -0.75$). It is noted that heat transfer rate $\left(Nu_x\,\mathrm{Re}_x^{-1/2}\right)$ decreases with viscous dissipation parameter Ec while increases as Prandtl number Pr increases from 0.7 to 7.0. For example, for $\alpha = 0.75$, *Ec* = 0.01, ε = 1.0, $A = 1.0$, Sc = 2.57, $\lambda = 1.0$ and ξ = 1.0 when τ = 0.5, heat transfer rate $\left(Nu_x\,\mathrm{Re}_x^{-1/2}\right)$ decreases approximately about 37% and 26% as Ec increases from -1.0 to 1.0 at Pr = 0.7 and at Pr = 7.0 (see Figure 13), respectively.

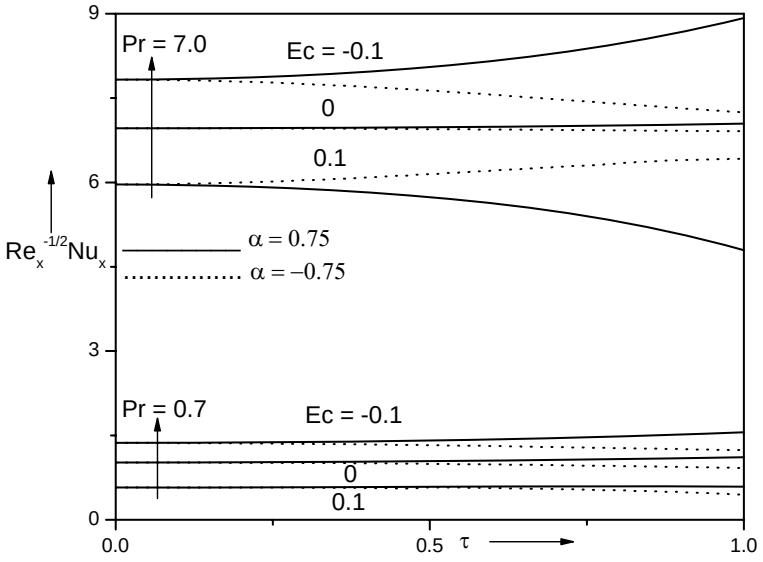

Figure 13. Effects of Pr and Ec on heat transfer rate for $\phi(\tau) = 1 + \alpha\tau^2$, when N = 0.5, λ = 2, ε = 1, Sc = 2.57, ξ = 1 and A = 1.

Moreover, it is noted that in the case of accelerating flows, the heat transfer rate $\left(Nu_x \operatorname{Re}_x^{-1/2}\right)$ increases with increasing time τ and $\left(Nu_x \operatorname{Re}_x^{-1/2}\right)$decreases with increasing time τ for the case of decelerating flows as can be seen in Figure 13.

Figure 14 displays the effects of the surface mass transfer $A\left(A>0 \text{ or } A<0\right)$ and viscous dissipation parameter *Ec* on the skin friction coefficient $\left(C_{fx} \operatorname{Re}_x^{1/2}\right)$ for accelerating and decelerating free stream flows ($\phi(\tau)=1+\alpha\tau^2$, $\alpha=0.75$ and $\alpha=-0.75$) when *N* = 1.0, ε = 1.0, *Pr* = 0.7, *Sc* = 2.57, $\lambda=1.0$ and ξ = 1.0. The skin friction coefficient$\left(C_{fx} \operatorname{Re}_x^{1/2}\right)$ increases noticeably as Eckert number *Ec* as well as surface mass transfer *A* increase. In particular, it is found for accelerating flow ($\alpha=0.75$) that the percentage decreases of $\left(C_{fx} \operatorname{Re}_x^{1/2}\right)$ by about 26% for τ = 0.5 at Ec = -1.0 and 1.0, respectively, as surface mass transfer *A* decreases from *A* = 0.0 to *A* = -1.5 while $\left(C_{fx} \operatorname{Re}_x^{1/2}\right)$ increases by about 22% and 21%, respectively at *Ec* = -1.0 and 1.0 when surface mass transfer *A* increases from *A* = 0.0 to *A* = 1.5. Further, it is also observed that $\left(C_{fx} \operatorname{Re}_x^{1/2}\right)$increases for heat generation (*Ec*>0) and decreases for heat absorption (*Ec* < 0).

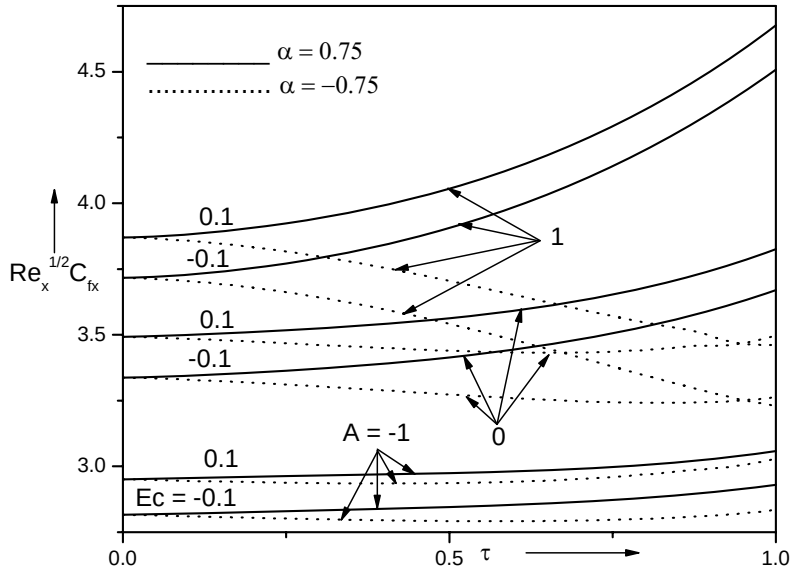

Figure 14. Effects of A and Ec on skin friction coefficient for $\phi(\tau)=1+\alpha\tau^2$, when ξ = 1, λ = 1, Sc = 2.57, N = 1, ε = 1 and Pr = 0.7.

It may be noted that the effect of suction or injection (*A*>0 or *A* < 0) is more prominent on skin friction coefficient. The effects of Schmidt number *Sc* and wall velocity parameter ε for accelerating and decelerating free stream flows ($\phi(\tau)=1+\alpha\tau^2$, $\alpha=0.75$ or $\alpha=-0.75$)

on the skin friction coefficient $\left(C_{fx}\,\mathrm{Re}_x^{1/2}\right)$ when Ec = 0.2, ε = 0.5, A = 1.0, N = 1.0, Pr = 0.7, $\lambda = 1.0$ and ξ = 1.0 are depicted in Figure 15.

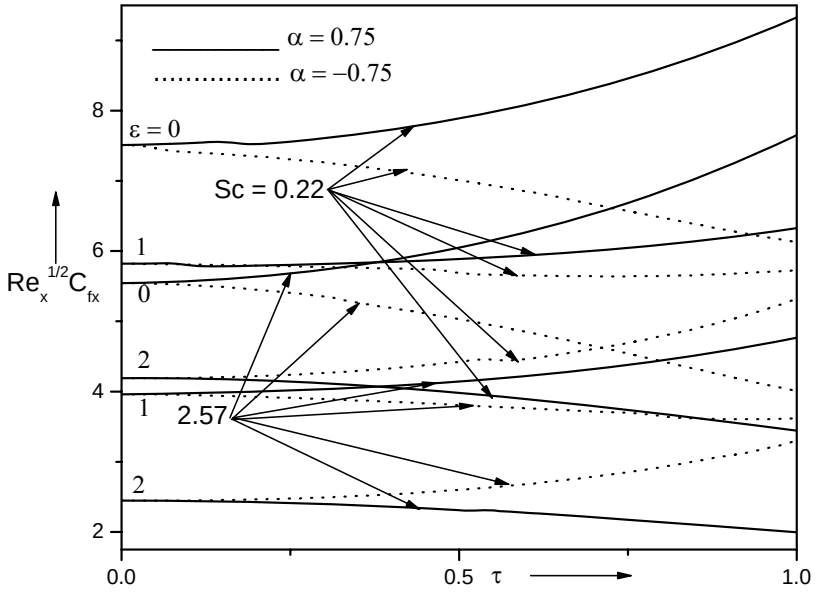

Figure 15. Effects of ε and Sc on skin friction coefficient for $\phi(\tau) = 1 + \alpha\tau^2$, when ξ = 1, λ = 1, N = 1, A = 1, Ec = 0.2 and Pr = 0.7.

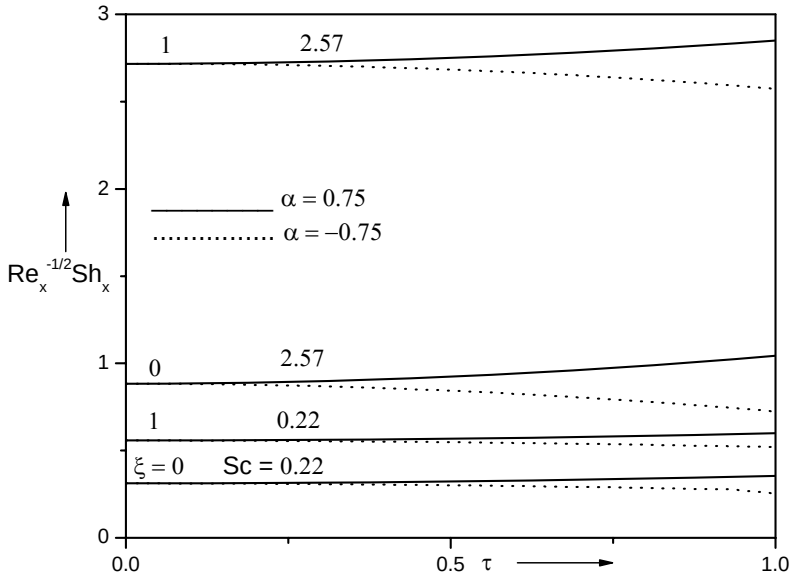

Figure 16. Effects of ξ and Sc on mass transfer rate for $\phi(\tau) = 1 + \alpha\tau^2$, when A = 1, λ = 1, Ec = 0.01, N = 1, ε = 1 and Pr = 0.7.

It is noted that when Schmidt number Sc increases from 0.22 to 2.57 as well as wall velocity parameter ε increases from 0 to 2, the skin friction coefficient $\left(C_{fx}\,\mathrm{Re}_x^{1/2}\right)$ decreases, as shown in Figs. 15. For example, for $\alpha = 0.75$, *Ec* = 0.2, N = 1.0, *A* = 1.0, Pr = 0.7, λ = 1.0 and $\xi = 1.0$ when τ = 0.5, $\left(C_{fx}\,\mathrm{Re}_x^{1/2}\right)$ decreases approximately about 23%, 30% and 42% as Sc increases from 0.22 to 2.57 at ε = 0.0, 1.0 and 2.0 (see Figure 15), respectively. Moreover, it is noted that in the case of accelerating flows, the skin friction coefficient $\left(C_{fx}\,\mathrm{Re}_x^{1/2}\right)$ increases remarkably with increasing time τ and $\left(C_{fx}\,\mathrm{Re}_x^{1/2}\right)$ decreases significantly with increasing time τ for the case of decelerating flows as can be seen in Figure 15.

Figure 16 displays the effects of the surface curvature parameter ξ and Schmidt number Sc on the mass transfer rate $\left(Sh_x\,\mathrm{Re}_x^{-1/2}\right)$ for accelerating and decelerating free stream flows ($\phi(\tau) = 1 + \alpha\tau^2$, $\alpha = 0.75$ and $\alpha = -0.75$) when *N* = 1.0, ε = 1.0, Pr = 0.7, *A* = 1.0, $\lambda = 1.0$ and ξ = 1.0. The mass transfer rate $\left(Sh_x\,\mathrm{Re}_x^{-1/2}\right)$ increases noticeably as surface curvature parameter ξ as well as Schmidt number Sc increase. In particular, it is found for accelerating flow ($\alpha = 0.75$) that the percentage increases of $\left(Sh_x\,\mathrm{Re}_x^{-1/2}\right)$ by about 186% and 384% for τ = 0.5 at ξ = 0.0 and 1.0, respectively, as Schmidt number increases from *Sc* = 0.22 to *Sc* = 2.57. Further, it is also observed that in the case of accelerating flows, the mass transfer rate $\left(Sh_x\,\mathrm{Re}_x^{-1/2}\right)$ increases steadily with increasing time τ and $\left(Sh_x\,\mathrm{Re}_x^{-1/2}\right)$ decreases remarkably with increasing time $\tau > 0.2$ approximately, for the case of decelerating flows as can be seen in Figure 16.

CONCLUSIONS

A numerical investigation is performed to study the unsteady mixed convection flow of a combined heat and mass transfer over a moving vertical slender. The unsteadiness is caused due to time dependent free stream velocity as well as moving slender cylinder velocity. Numerical results indicate that the buoyancy force (λ) and the ratio of buoyancy forces (N) enhance the skin friction coefficient and local Nusselt number. From the figures, it is found that in presence of buoyancy force $(\lambda > 0)$ and the ratio of buoyancy forces (N), the velocity profile exhibits velocity overshoot 70% more for lower Prandtl number as compared to the magnitude of the velocity overshoot for higher Prandtl number. For a fixed buoyancy force, the coefficient of skin friction decreases with Prandtl number while local Nusselt number increases. Also, an increase in the Prandtl number results into a strong reduction up to 45 % in the thickness of the thermal boundary layer. Further, an increase in the Schmidt number Sc leads to a strong reduction up to 60% in the concentration boundary layer. The effect viscous dissipation leads to a rise in the momentum and thermal boundary layers. Profiles in graphs display that the time dependent free stream velocity has 40 % more effect

on the velocity profiles as compared to the corresponding temperature and concentration profiles.

ACKNOWLEDGMENTS

The authors wish to express their thanks to the anonymous reviewers for their valuable comments and suggestions. Dr. P. M. Patil is thankful to the University Grants Commission, South Western Regional Office, Bangalore, India, for the financial assistance under the Minor Research Project No. MRP(S)-636/09-10/KAKA060/UGC-SWRO. Also, Dr. Patil is dedicated this paper to one of his close friends Shri B. L. Hosamani, Assistant Commissioner of Commercial Taxes, Government of Karnataka, India, who recently passed away in road accident.

APPENDIX

$$X_1^{\,i}=(1+\xi\eta)^{-1}\left[\xi+\phi\left(f+\xi f_\xi\right)\right];\ X_2^{\,i}=-(1+\xi\eta)^{-1}\left[\frac{\xi^2}{4}\phi^{-1}\frac{d\phi}{d\tau}+\phi\xi F_\xi\right];$$

$$X_3^{\,i}=-(1+\xi\eta)^{-1}\phi\xi F;\ X_4^{\,i}=-(1+\xi\eta)^{-1}\frac{\xi^2}{4};\ X_5^{\,i}=(1+\xi\eta)^{-1}8\phi^{-1}\lambda; \qquad (A_1)$$

$$X_6^{\,i}=(1+\xi\eta)^{-1}8\phi^{-1}\lambda N;\ X_7^{\,i}=-\xi(1+\xi\eta)^{-1}\left[\phi F F_\xi+\frac{\xi}{2}\phi^{-1}\frac{d\phi}{d\tau}\right];$$

$$Y_1^{\,i}=(1+\xi\eta)^{-1}\left[\xi+\Pr\phi\left(f+\xi f_\xi\right)\right];$$

$$Y_2^{\,i}=-(1+\xi\eta)^{-1}\Pr\phi\xi F;\ Y_3^{\,i}=-(1+\xi\eta)^{-1}\Pr\frac{\xi^2}{4};\ Y_4^{\,i}=-(1+\xi\eta)^{-1}\Pr\phi\xi G_\xi \qquad (A_2)$$

$$Y_5^{\,i}=2\Pr Ec\phi^2 F_\eta;\ Y_6^{\,i}=\Pr Ec\phi^2 F_\eta^{\,2}-(1+\xi\eta)^{-1}\Pr\xi\phi G_\xi F;$$

$$Z_1^{\,i}=(1+\xi\eta)^{-1}\left[\xi+Sc\phi\left(f+\xi f_\xi\right)\right];\ Z_2^{\,i}=-(1+\xi\eta)^{-1}Sc\phi\xi F;$$

$$Z_3^{\,i}=-(1+\xi\eta)^{-1}Sc\frac{\xi^2}{4};\ Z_4^{\,i}=-(1+\xi\eta)^{-1}Sc\phi\xi H_\xi;$$

$$Z_5^{\,i}=-(1+\xi\eta)^{-1}Sc\xi\phi H_\xi F\ . \qquad (A_3)$$

REFERENCES

[1] D. Anilkumar, S. Roy, Self-similar solution of the unsteady mixed convection flow in the stagnation point region of a rotating sphere, *Heat Mass Transfer* 40 (2004) 487 – 493.

[2] S. Roy, D. Anilkumar, Unsteady mixed convection from a rotating cone in a rotating fluid due to the combined effects of thermal and mass diffusion, *International Journal of Heat Mass Transfer,* 47 (2004) 1673 – 1684.
[3] D. Anilkumar, S. Roy, Unsteady mixed convection flow on a rotating cone in a rotating fluid, *Applied Mathematics and Computation* 155 (2004) 545 – 561.
[4] T.S. Chen, A. Mucoglu, Buoyancy effects on forced convection along a vertical cylinder, *ASME J. Heat Transfer*, 97 (1975) 198 -203.
[5] Mucoglu, T.S. Chen, Buoyancy effects on forced convection along a vertical cylinder with uniform heat flux, *ASME J. Heat Transfer*, 98 (1976) 523 -525.
[6] M.N. Bui, T. Cebci, Combined free and forced convection on vertical slender cylinders, *ASME J. Heat Transfer* 107 (1985) 476 -478.
[7] S.L. Lee, T.S. Chen, E.F. Armaly, Mixed convection along a vertical cylinders and needles with uniform surface heat flux, *ASME J. Heat Transfer* 109 (1987) 711 -716.
[8] T.Y. Wang, C. Kleinstruver, General analysis of steady mixed convection heat transfer on vertical slender cylinders, *ASME J. Heat Transfer* 111 (1989) 393 -398.
[9] H.S. Takhar, A.J. Chamkha, G. Nath, Combined heat and mass transfer along a vertical moving cylinder with a free stream, *Heat Mass Transfer* 36 (2000) 237 -246.
[10] J.J. Heckel, T.S. Chen, B.F. Armaly, Mixed convection along slender vertical cylinders with variable surface temperature, *Int. J. Heat Mass Transfer* 32 (1989) 1431 – 1442.
[11] M. Kumari, G. Nath, Mixed convection boundary layer flow over a thin vertical cylinder with localized injection/suction and cooling/heating, *Int. J. Heat Mass Transfer* 47 (2004) 969 – 976.
[12] E.M. Sparrow, H.S. Yu, Local non-similarity thermal boundary layers, *ASME J. Heat Transfer* 93 (1971) 328 -334.
[13] S. Roy, D. Anilkumar, Unsteady mixed convection from a moving vertical slender cylinder, *ASME J. Heat Transfer* 128 (2006) 368 -373.
[14] P.J. Singh, S. Roy, I. Pop, Unsteady mixed convection from a rotating vertical slender cylinder in an axial flow, *Int. J. Heat Mass Transfer* 51 (2004) 1423 – 1430.
[15] K. Inouye, A. Tate, Finite difference version quasilinearisation applied to boundary layer equations, *AIAAJ* 12 (1974) 558- 560.
[16] H. Schlichting, *Boundary layer theory*, Springer, New York, 2000.
[17] Pop, D. B. Ingham, *Convective heat transfer: Mathematical and Computational Modelling of Viscous Fluids and Porous Media*, Pergman, Oxford, 2001.
[18] R.S. Varga, *Matrix Iterative Analysis*, Prentice Hall, Englewood Cliffs, NJ 2000.

Received 29 October 2010, received in revised form 25 August 2011, accepted 30 August 2011.